LAWRENCE
LIVERMORE
NATIONAL
LABORATORY

UCRL-CONF-216523

A System for Measuring Defect Induced Beam Modulation on Inertial Confinement Fusion-class Laser Optics

M. Runkel, R. Hawley-Fedder, C. Widmayer, W. Williams, C. Weinzapfel, D. Roberts

October 25, 2005

Boulder Damage Symposium
Boulder, CO, United States
September 19, 2005 through September 21, 2005

A system for measuring defect induced beam modulation on inertial confinement fusion-class laser optics

Mike Runkel*, Ruth Hawley-Fedder, Clay Widmayer, Wade Williams, Carolyn Weinzapfel, Dave Roberts
Lawrence Livermore National Laboratory, 7000 East Avenue, Livermore, California 94551

ABSTRACT

A multi-wavelength laser based system has been constructed to measure defect induced beam modulation (diffraction) from ICF class laser optics. The Nd:YLF-based modulation measurement system (MMS) uses simple beam collimation and imaging to capture diffraction patterns from optical defects onto an 8-bit digital camera at 1053, 527 and 351 nm. The imaging system has a field of view of 4.5 x 2.8 mm^2 and is capable of imaging any plane from 0 to 30 cm downstream from the defect. The system is calibrated using a 477 micron chromium dot on glass for which the downstream diffraction patterns were calculated numerically. Under nominal conditions the system can measure maximum peak modulations of approximately 7:1. An image division algorithm is used to calculate the peak modulation from the diffracted and empty field images after the baseline residual light background is subtracted from both. The peak modulation can then be plotted versus downstream position. The system includes a stage capable of holding optics up to 50 pounds with x and y translation of 40 cm and has been used to measure beam modulation due to solgel coating defects, surface digs on KDP crystals, lenslets in bulk fused silica and laser damage sites mitigated with CO_2 lasers.

Keywords: optical defect, beam intensification, diffraction

1. INTRODUCTION

The diffraction patterns produced by obscurations to a light beam are of central importance to the development of optics.[1,2] Many diffraction-based measurement systems have been built to investigate a broad range of phenomena including particle sizing applications, wire diameter measurements[3-6] and for verification of the predictions of diffraction theory and improvement of numerical beam propagation calculations.[7-9] Despite this, the number of diffraction-based measurements systems constructed to characterize "common" optical defects such as scratches and digs is few[10] and published studies of these defects are rare.[11] From the standpoint of megajoule-class inertial confinement fusion (ICF) lasers, such as the National Ignition Facility (NIF),[12] it is important to understand the diffraction behavior of these defects for a number of reasons. The first is to assess the risk of optical damage by direct intensity enhancement to the (sometimes) tightly-packed component modules of these lasers. This will also impact the optic lifetime and the shot fluences and sequences to which the optics will be exposed. The second is to understand the contribution of diffraction to the overall phase perturbations/non-uniformities of the beam (the B integral) that may lead to beam breakup, self focusing and damage to downstream optical components and other performance issues.[13,14] The third issue is to provide real-world input into the beam propagation programs such as PROP[15] so that modelers may better predict laser performance under the wide variety of shot conditions expected for ICF class lasers.

For megajoule-class laser systems such as the NIF there will be in excess of 20,000 precision, large aperture (>40cm) optical components. These components include laser glass slabs, polarizers, transport mirrors, Pockel's cell and frequency conversion crystals, focus lenses along with a variety of vacuum windows, beam separation gratings and phase plates. Each of these optic types and its particular coating must meet a stringent set of specifications designed to optimize its performance within the laser beam line. Nevertheless, because of the size of the optics and number that must be produced it is inevitable that certain types and numbers of defects will occur. The principle defects of interest are agglomerations of solgel from the AR coating process, surface digs on KDP crystals that arise from the finishing process, bulk lenslets (refractive index inhomogeneites) found in fused silica as well as mitigated and unmitigated surface laser damage sites.[16]

* e-mail runkel1@llnl.gov; phone 925-424-2210

2. SYSTEM REQUIREMENTS

Conceptually, measuring the diffraction pattern of the optical defect is relatively straightforward. The defect needs to be exposed to a uniform, collimated laser source and the diffraction image captured at the downstream plane of interest for later analysis. In practice a number of considerations influence the design of this modulation measurement system (MMS). For ICF-class optics the system must be capable of handling a variety of large optics weighing up to 50 lbs. It must also be simple to operate and obtain pass/fail information in real time. It must be robust, requiring little adjustment over long periods of time as well as be easily maintained and converted between wavelengths.

Because of the wide variety of defects of interest, particularly the solgel coating defects, a commercially available Nd:YLF multi-wavelength system providing measurement capability at the use wavelength of each optic was used. The 1053 nm (1ω) laser is acousto-optically q-switched and operated at 5 KHz. It also simultaneously emits second and third harmonics at 527 nm (2ω) and 351 nm (3ω). Referring to Figure 1, the wavelength of interest is selected by an appropriate narrow-line laser wavelength pass filter (WF). The laser is then spatially filtered using a 25 micron pinhole (SF) and collimated using an uncoated 1 meter fused silica lens (L1). The up-collimated beam is delivered to the test piece using a variety of protected aluminum turning mirrors (M3-M6) including a periscope because of lab space constraints. The final turning mirror (DM) is a dielectric, 45 degree high reflector with wavelength specific coating. A green HeNe beam is passed through the back of this mirror to act as a visible alignment source for the collimated beam. After passing through the sample under test the beam and resulting diffraction pattern are imaged onto a digital, 8-bit CCD camera using an uncoated 100 mm focal length fused silica lens (L2) with diameter of 50 mm. The collimating and imaging lenses are uncoated to accommodate rapid conversion between wavelengths. The system magnification has been set to provide a nominal spatial resolution of 6 microns/pixel which is 1.8 times better than that used LLNL's beam PROP codes. The entire lens/camera system is mounted on a 30-cm translation stage and moved along the propagation axis to sample the diffraction pattern in space. This assembly is also enclosed in a black-anodized aluminum box to reduce stray room light and the system is operated without room lights. The images are captured and stored in TIFF format for later analysis. The X and Y sample stages are capable of 40 cm travel allowing the entire clear aperture of the optics to be examined. The stages are also capable of handling samples weighing up to 50 lbs.

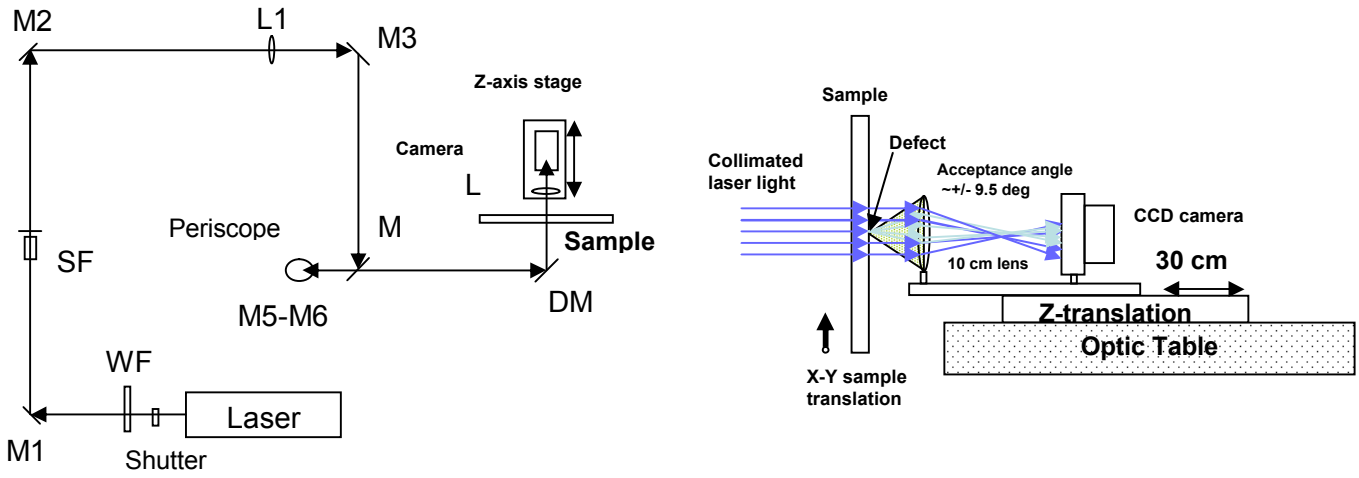

Figure 1. Schematic of the optical layout for the modulation measurement system (MMS). The left hand side shows the overall system layout while the right hand side shows the left hand side view of the system.

3. SYSTEM CALIBRATION AND PERFORMANCE

Prior to any testing, the baseline laser intensity is set to give an average of approximately 50 counts (out of 256) with no defect in the field of view when the ambient light background was subtracted from the image. When operated with this number of counts, the system dynamic range is approximately 5:1 before pixel saturation. With room lights off a residual 12-14 count background is present. The system was calibrated using a test pattern consisting of a 477 micron diameter chromium dot that had been vacuum deposited on a glass substrate. At each wavelength the diffraction patterns at 0-7 cm in 1 cm increments, 10 cm and 20 cm were captured and compared to PROP calculations. Line outs through the images showed good agreement with

the numerical calculations when appropriate background counts were subtracted (see Figure 2) and comparison of 1ω, 2ω and 3ω images at 2, 4 and 6 cm object planes confirmed the λz wavelength scaling expected from diffraction theory.[2]

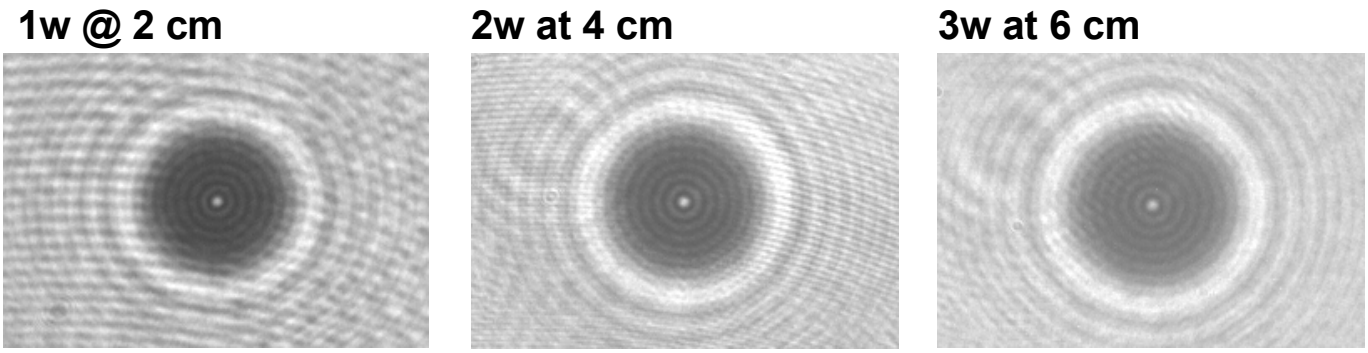

Figure 2. Raw images of the diffraction from a 477 μm dot at 1053 nm, 2 cm, 527 nm, 4 cm and 351 nm, 6 cm from focus respectively. These images were used to verify the wavelength scaling predicted by the Huygens-Fresnel integral as part of MMS system characterization.

As can be seen in Figures 2 and 3 there is a significant amount of beam ripple that is present in the images, particularly at 1ω. This is due to interference from the uncoated collimating and imaging lenses. At 1ω this contributes noise on the order of 40 percent.

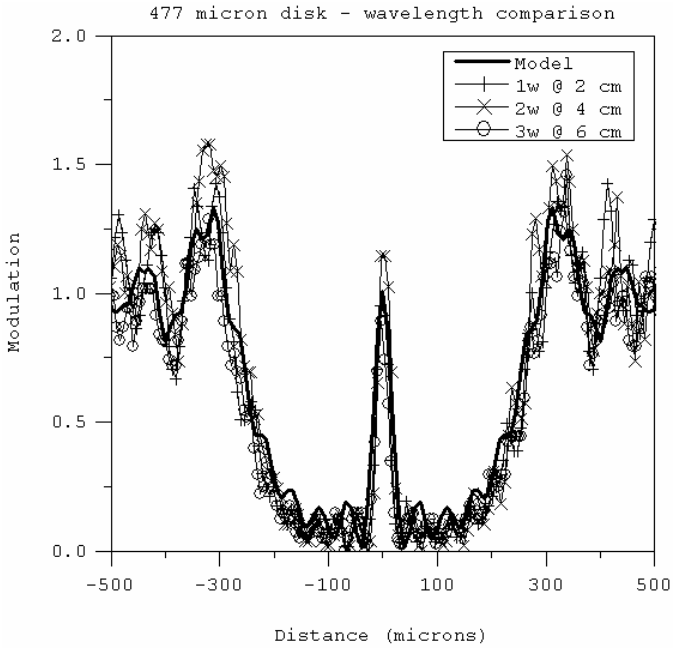

Figure 3. Vertical lineouts taken through the center of the images of Figure 2 and compared to the PROP model results for 351 nm at 6 cm. Outside of the obscured region there is significant noise on the data.

For data to be useful this level of noise must be eliminated. The most effective way is to generate the modulation image (M) by subtracting off the ambient light background (B) from the diffracted (disturbed) field image (D_{meas}) and its associated empty field image (F_{meas})(where the defect was moved out of the field of view), then dividing the corrected diffracted image (D) by the corrected empty field image (F) on a pixel-by-pixel basis to get the modulation. This process is described by the equation

$$M = \frac{D}{F} = \frac{D_{meas} - B}{F_{meas} - B} \tag{1}$$

After the modulation conversion algorithm is applied the resulting image is searched for the highest value. This analysis is repeated on a sequence of downstream images allowing the peak modulation as a function of propagation distance to be determined. The effect of image processing on a solgel coating agglomeration at 1ω is shown in Figure 4.

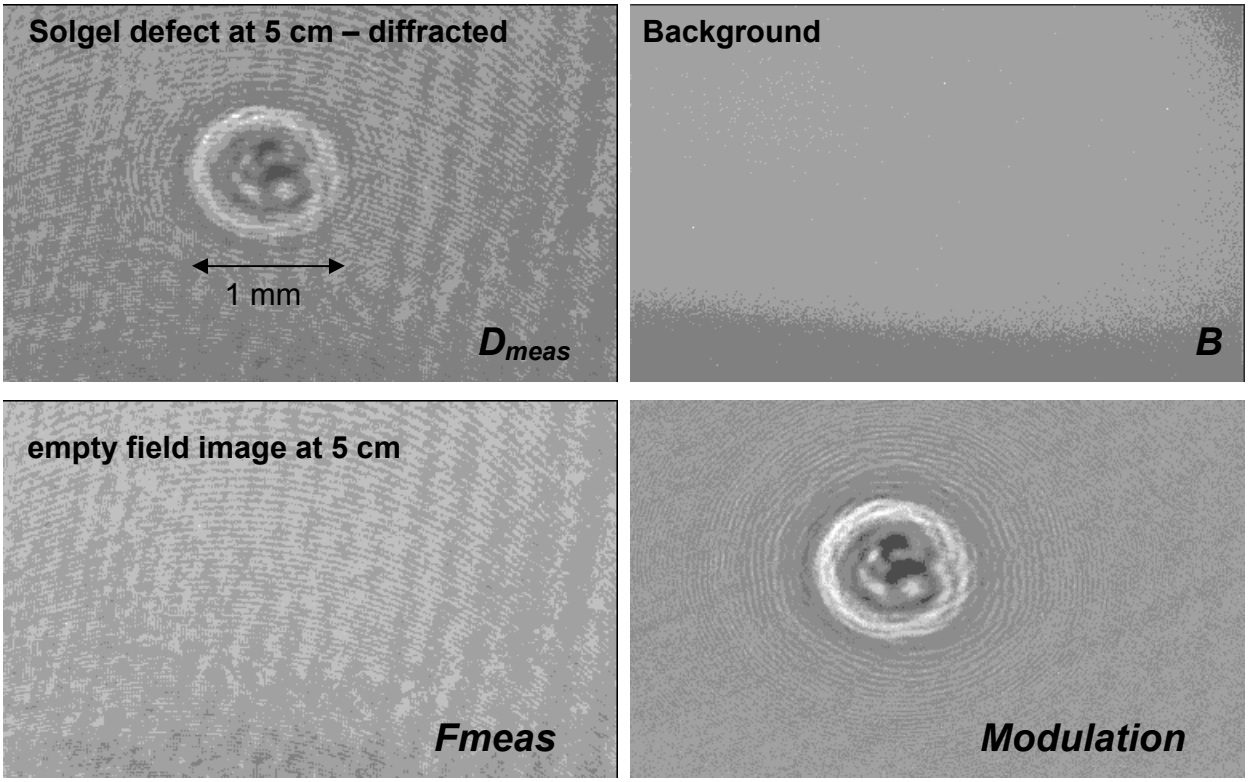

Figure 4. MMS images showing the process of noise elimination using the image division algorithm.

The method reduces the background noise to approximately 5% (rms) and is highly effective at extracting diffraction data from the noise. Figure 5 shows how a coating defect is revealed from the raw image by the modulation algorithm.

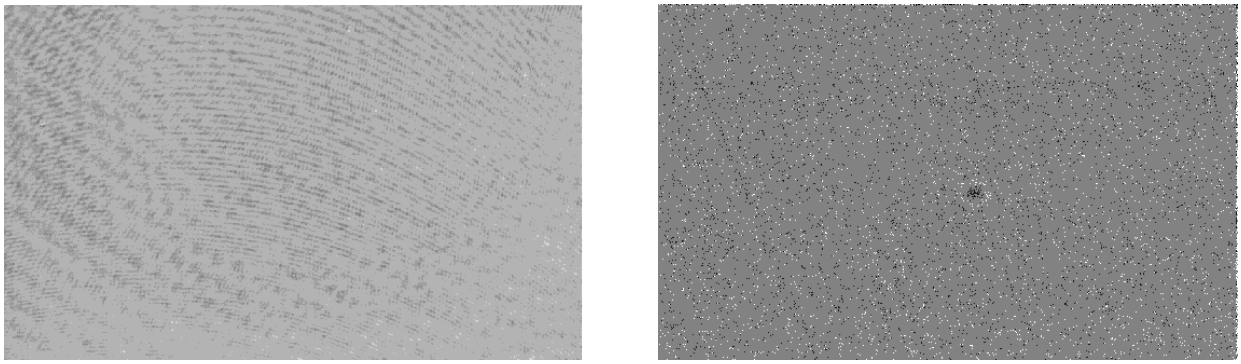

Figure 5. Raw and processed images of a solgel coating defect on a KDP crystal. These images illustrate the ability of the image processing method to reveal subtle defects on the sample.

4. MEASUREMENTS ON OPTICAL DEFECTS

In this section the results of measurements on a variety of defects that have been found on ICF-class laser optics are presented. Figure 6 shows how the modulation evolves as the 3ω light propagates away from a 50 micron pinpoint solgel coating defect on a KDP tripler crystal.

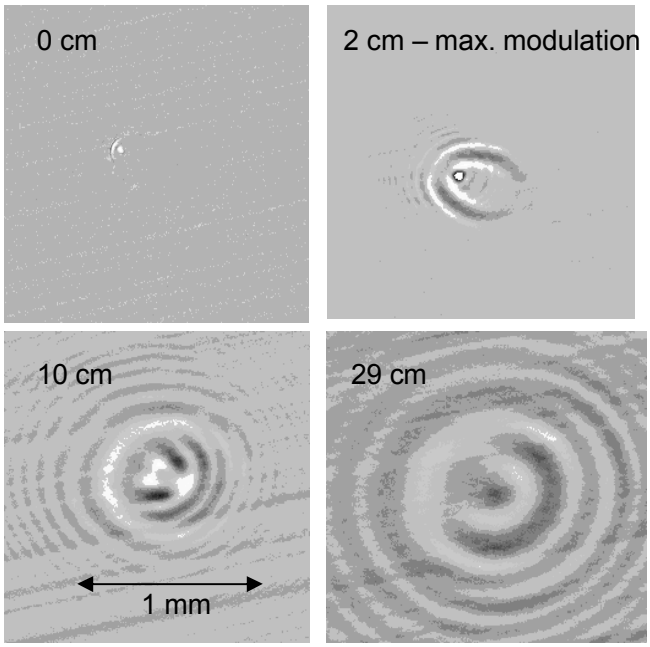

Figure 6. The evolution of beam modulation from a small solgel coating defect on KDP. The central spot in the upper left image (0 cm) is approximately 15 μm wide. Not shown in that image is a locally disrupted region of approximately 500 μm. This region is revealed in subsequent downstream images, particularly at 2 cm where the peak intensity is at a maximum of 6.9:1 for downstream propagation.

This defect is surrounded by a 0.5 mm diameter region where the solgel coating was disrupted on the optic surface. At focus (0 cm) only the poinpoint can be seen in the image. As the light propagates downstream the modulation peaks with a value of 6.9 at 2 cm and gradually falls off to below approximately 3:1 beyond 10 cm (see Figure 7).

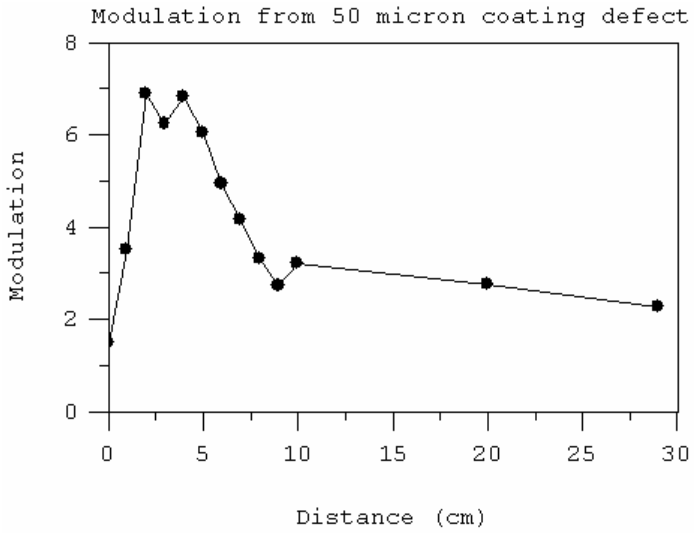

Figure 7. The modulation vs. distance plot for the solgel defect shown in Figure 6. The intensification peaks at 6.9:1 only 2 cm from the sample surface.

Figure 8 shows the modulation evolution from 0 to 20 cm for a 725 micron wide by 160 micron deep CO_2 laser-drilled pit having a gaussian depth profile. The FWHM for this pit was approximately 550 microns. Modulations approaching 4:1 have been measured on the lip of the crater at focus. The peak modulation generally falls off to no more than 2.5:1 at 3 cm and occurs outside the physical region of the pit. It then starts increasing and reaches its maximum in the region of 4-7 cm downstream from the focus. The peak no longer occurs outside the physical dimension of the crater, but rather inside it.

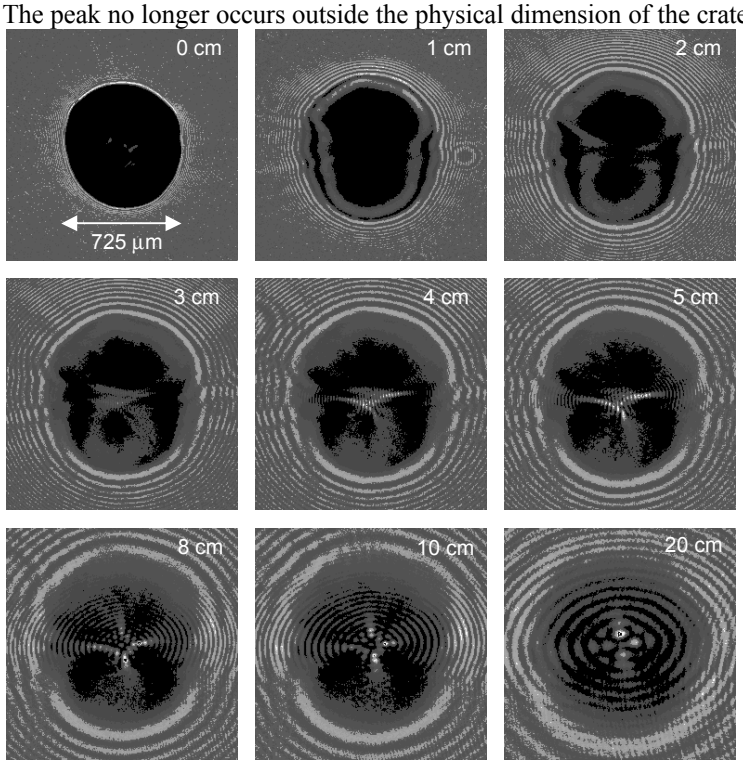

Figure 8. The evolution of modulation from a CO_2 laser drilled pit in fused silica. The nominal surface diameter of the pit is ~725 µm. The Gaussian profile of the pit leads to scattering of much of the light at high angles that are outside the acceptance angle of the MMS. This causes the pit to appear dark.

Measurements on a number of nominally identical laser-drilled pits show significant variation in the shape of the modulation curve with a value of 4.8:1 being the highest observed. The modulation curves for 4 individual laser pits are shown in Figure 9.

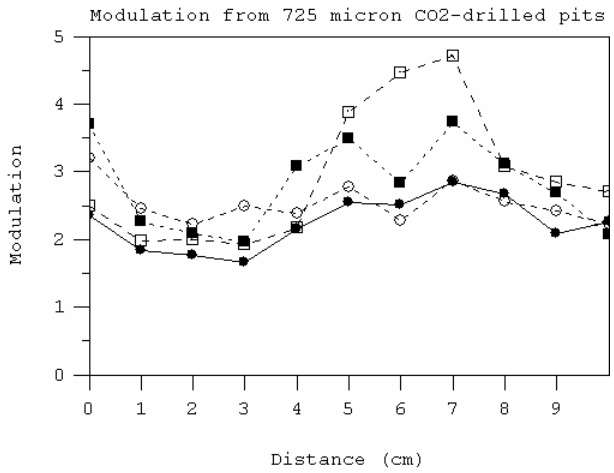

Figure 9. The modulation vs. position curve for 4 CO_2 laser-drilled pits in fused silica. The pits were drilled under nominally identical condition including exposure time and laser power and show significant variation in the level of peak modulation produced by the geometry.

The modulation behavior of two surface digs on a KDP tripler crystal is shown in Figures 10 and 11. The dig shown in Figure 10 is quite large. The 0-cm image (upper left) shows the large surface cracks extending vertically (~600 microns) and a longer, narrower crack propagating along a weak crystalline axis in the horizontal direction. The crack network also extends below the surface and is indicated by the approximately 500 micron diameter dark central portion of the image.

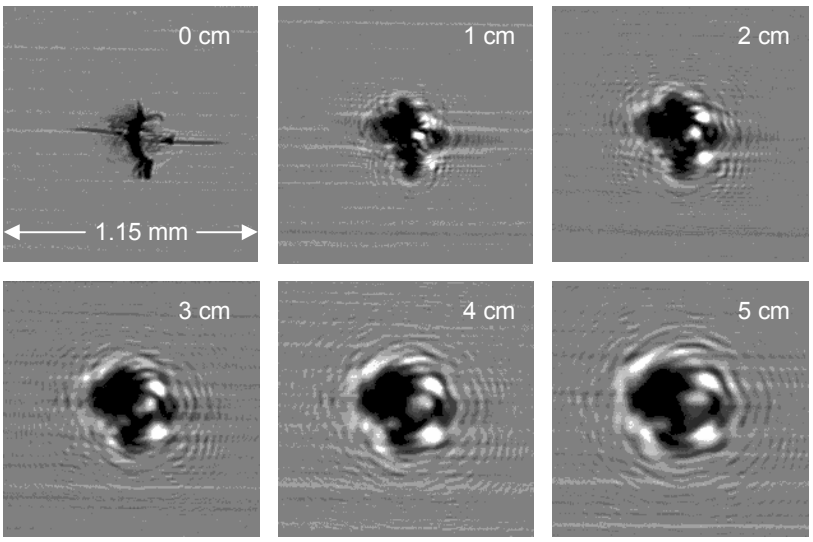

Figure 10. Beam modulation from a large surface dig on a KDP tripler crystal. Note the large crack network in the upper left image.

The modulation pattern develops rapidly peaking at 3.7:1 at only 2 cm downstream from the sample surface. The diffraction from the narrow horizontal crack disappears by 3 cm from focus where the basic far-field diffraction pattern has formed. This pattern does not change significantly from 5 cm to 28 cm downstream and the modulation drops from 3.1:1 to 2.1:1 over this range. The smaller, 50 x 150 μm^2 dig shown in Figure 11 exhibits similar behavior but exhibits a much lower overall modulation as shown in Figure 12. The modulation peaks at 2.2:1 at only 1 cm from focus. After reaching the far-field at 4 cm from focus, the modulation drops from 1.7:1 to 1.4:1 at 28 cm.

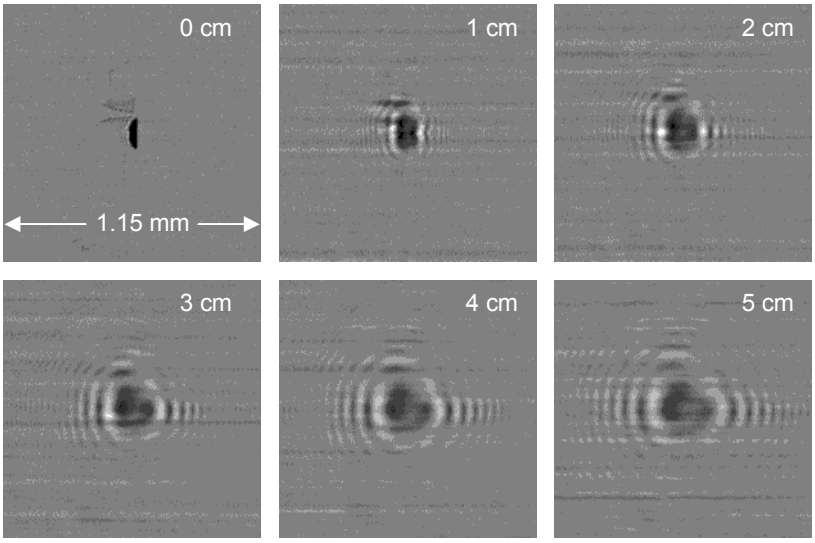

Figure 11. Beam modulation from a small surface dig on a KDP tripler crystal. Note that the overall intensification is significantly lower for the small defect compared to the larger one with its network of cracks.

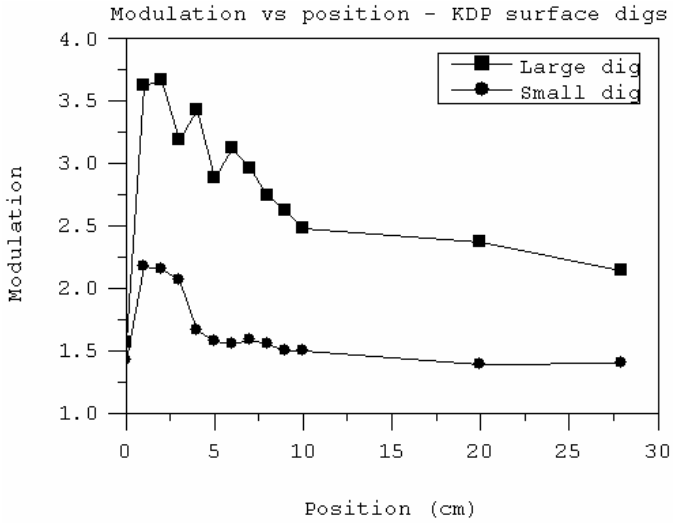

Figure 12. The modulation vs. distance curves for the KDP surface digs shown in Figures 10 and 11. The smaller dig has much lower overall beam intensification than the large dig and reaches its far-field modulation level 5 cm sooner than the large dig.

5. Conclusion

A laser-based modulation measurement system has been constructed and calibrated for the measurement of diffraction from common optical defects found on ICF-class laser optics. The MMS system has been used to characterize solgel coating agglomerations, laser-drilled pits and crystal surface digs. Maximum modulations approaching 7:1 have been measured for small coating defects (<50 microns) within 4 cm of the sample surface. Ensembles of large laser-drilled pits in fused silica have exhibited modulation exceeding 4.5:1 from 5-7 cm from the sample surface. For KDP surface digs the measurements indicate that larger overall size causes higher maximum modulations. The diffraction from cracks present with these digs dissipates quickly as the beam propagates downstream. Modulation curves generated from these defects will be used to assess the risk of components to optical damage and to improve the predictive power of computer models such as PROP.

ACKNOWLEDGMENTS

This work has been performed under the auspices of the U.S. DOE by UC, LLNL contract number W-7405-ENG-48.

REFERENCES

1. M. Born, E. Wolf, *Principles of Optics, 6th Edition* (Pergamon Press, Oxford, England, 1993)
2. J. Goodman, *Introduction to Fourier Optics* (McGraw-Hill, San Francisco, CA, 1968)
3. Z. Ma, H. G. Merkus, B. Scarlett, "Extending Laser Diffraction for Particle Shape Characterization: Technical Aspects and Application," Powder Technology 118, 180-187 (2001)
4. Z. Ma, H. G. Merkus, B. Scarlett, "Particle-size Analysis by Laser Diffraction with a Complementary Metal-Oxide Semiconductor Pixel Array, Applied Optics, **39**(25), 4547-4556 (2000)
5. T. Mou, X. Zhou, "The Methods of Laser Diffraction Measurement for Non-spherical Particles, *Advanced Photonic Sensors: Technology and Applications*, J. Tang, C. Xu, H. Li, Editors, Proceedings of SPIE Vol. 4220, 269-272 (2000)
6. D. Lebrun, S. Belaid, C. Oezkul, K. Ren, G. Grehan, "Enhancment of Wire Diameter Measurements: Comparison Between Fraunhofer Diffraction and Lorenz-Mie Theory," Optical Engineering, **35**(4), 946-950 (1996)
7. R. Duogang, "Study on Laser Diffraction Measurement," *Automated Optical Inspection for Industry: Theory, Technology, and Applications II,* Proceedings of SPIE Volume 3558, 201-208 (1998)
8. R. English, N. George, "Diffraction patterns in the shadows of disks and obstacles," Applied Optics, 27(8), 1581-1587 (1988)

9. A. Mahan, C. Bitterli, S. Cannon, “Far-field Diffraction Patterns of Single and Multiple Apertures Bounded by Arcs and Radii of Concentric Circles,” J. Opt. Soc. of Am., 54(6), 721-732 (1964)
10. D. Smith, “The Development of Ion-Etched Phase Plates,” LLE Review, Quarterly Report, Volume 74, 71-91 January-March 1998, DOE/SF/19460-241
11. P. Klingsporn, “Deteremination of the Diameter of an Isolated Surface Defect Based on Fraunhofer Diffraction,” Applied Optics, 19(9), 1435-1438 (year)
12. E. M. Campbell, “The National Ignition Facility project,” Fusion Technology, 26, 755-766 (1994)
13. W. Williams, K. Manes, J. Hunt, P. Renard, D. Milam, D. Eimerl, “Modeling of Self-Focusing Experiments by Beam Propagation Codes,” UCRL-LR-105821-96-1, ICF Quarterly Report, Lawrence Livermore National Laboratory (1996)
14. M. Shaw, W. Williams, R. House, C. Haynam, “Laser Performance Operations Model,” Optical Engineering, 43(12), 2885- 2895 (2004)
15. R. Sacks, M. Hensian, S. Haney, J. Trenholme, “The PROP92 Fourier Beam Propagation Code,” ICF Annual Report, CRL-LR-105821-96, 207- 216 (1996)
16. M. Feit, A. Rubenchik, “Mechanisms of CO_2 Laser Mitigation of Laser Damage Growth in Fused Silica,” Laser Induced Damage in Optical Materials: 2002, Proceedings of SPIE, Volume 4932, 91-102 (2003)